# Electronic Supplemental Information

Decoupling the optical and electrical properties of subphthalocyanine/$C_{70}$ bi-layer organic photovoltaic devices: improved photocurrent while maintaining a high open-circuit voltage and fill factor

Chih-Chien Lee,[a]* Wei-Cheng Su,[a] Yi-Sheng Shu,[b] Wen-Chang Chang,[a] Bo-Yao Huang,[a] Ya-Ze Lee,[b] Tsung-Hao Su,[b] Kuan-Ting Chen[a] and Shun-Wei Liu[b]*

[a]Department of Electronic Engineering, National Taiwan University of Science and Technology, Taipei 10607, Taiwan, Republic of China
[b]Department of Electronic Engineering, Ming Chi University of Technology, New Taipei City 24301, Taiwan, Republic of China

## S1. Diode properties of OPV devices

In a conventional OPV device based on a p-n junction, the *J-V* curve can be approximated by the equivalent circuit model[1]

$$J = \frac{1}{1+R_S/R_{SH}} \left\{ J_0 \left[ \exp\left( \frac{V-JR_SA}{nkT/q} \right) - 1 \right] - \left( J_{PH} - \frac{V}{R_{SH}A} \right) \right\}, \tag{1}$$

where $R_S$ and $R_{SH}$ are the series and shunt resistance, respectively, *A* is the device active area, $J_{PH}$ is the photocurrent, *kT* is the thermal energy, *q* is the elementary charge, $J_0$ and *n* denotes the reverse saturation current and the ideality factor of the diode, respectively. In the dark, the $J_{PH}$ is equal to 0, thus yields the theoretical expression of the dark current. However, the natures of amorphous and trap-riched properties in the organic semiconductors render the organic-based heterojunction devices sometimes failed to the theoretical prediction, especially in the dark current.[2, 3] These deviations were generally observed under a high reverse and/or low forward bias. At a reverse bias, the ideal diode turned off and shows a low saturation current, while the organic devices may exhibit a monotonically increased current because of either the trap present in the bulk or at organic/metal interface.[2] This phenomenon is more significant in the high reverse bias, which indicates the current is favored by electrical field that increases the possibility of carrier hopping between organic molecules.

These traps may also contribute to the deviation in a low forward bias because of thermally activated current injection. Because the trap-induced current can be regarded as the leakage current, which is related to the $R_{SH}$ of the diode, we simply assume that the $R_{SH}$ is voltage-dependent and can be express as $R_{SH0} \pm \beta V R_{SH0}$, where $\beta$ represents the trap dependence and the sign depends on the polarity of the applied bias. This simple approximation is only valid when $V$ is between -1 to 1.5 V. The physical meaning of this expression and its deficiency are beyond the scope of the current study but will be further developed in our on-going research. By applying Eq. (1) in combination to our assumption, the experimental dark currents of OPV devices with varied $C_{70}$ thicknesses were in good agreement with the theoretical prediction as shown in Fig. S1. The extracted diode parameters are summarized in Table S1. Note that the $\beta$ was 0.7 for all the devices. All the diode parameters were generally identical except the $R_S$ for the 10 nm device, indicating the unchanged diode behavior when the $C_{70}$ thickness was increased. To further verify the diode properties under an AM 1.5G solar illumination, we also perform the same calculation with $J_{PH} = J_{SC}$ in Eq. (1). Fig. S2 shows the experimental and calculated photocurrents for all the devices. The fitting parameters are summarized in Table S2, showing the similar values for $n$, $J_0$, and $R_S$ to the results obtained in the dark. However, a very different $R_{SH}$ was obtained, which is usually changed under illumination because of an enhanced carrier recombination. These results further confirm that the electrical property is almost independent of the $C_{70}$ film thickness.
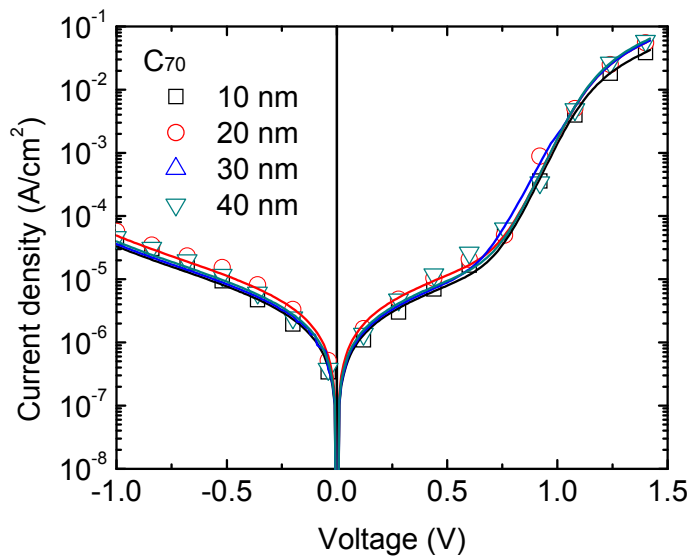


Fig. S1. Dark currents of the OPV devices with varied $C_{70}$ thicknesses in the structure of

ITO/MoO$_3$ (15 nm)/SubPc (10 nm)/C$_{70}$/BCP (8 nm)/Ag (100 nm). Solid lines are the corresponding fits.

Table S1. Diode parameters by fitting the experimental dark current to Eq. (1) with a modified $R_{SH}$.

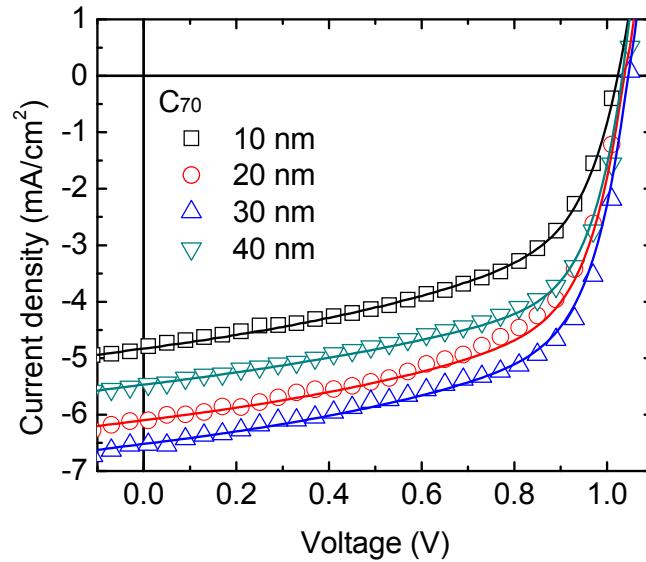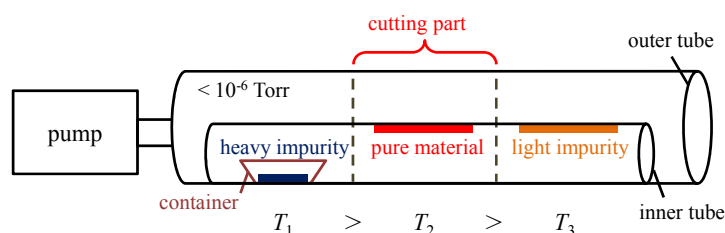| Device | $n$ | $J_0$ (A/cm$^2$) | $R_S$ ($\Omega$) | $R_{SH0}$ ($\Omega$) |
|--------|-----|------------------|------------------|----------------------|
| 10 nm | 2.2 | 4.30 x 10$^{-11}$ | 145 | 2500000 |
| 20 nm | 2.2 | 4.90 x 10$^{-11}$ | 96 | 1700000 |
| 30 nm | 2.2 | 4.80 x 10$^{-11}$ | 95 | 2300000 |
| 40 nm | 2.2 | 5.00 x 10$^{-11}$ | 88 | 2100000 |



Fig. S2. Photocurrents of the OPV devices with varied C$_{70}$ thicknesses in the structure of ITO/MoO$_3$ (15 nm)/SubPc (10 nm)/C$_{70}$/BCP (8 nm)/Ag (100 nm). Solid lines are the corresponding fits.

Table S2. Diode parameters by fitting the experimental photocurrent to Eq. (1) with a modified $R_{SH}$ and $J_{PH} = J_{SC}$.

| Device | $n$ | $J_0$ (A/cm$^2$) | $R_S$ ($\Omega$) | $R_{SH0}$ ($\Omega$) |
|--------|-----|------------------|------------------|----------------------|
| 10 nm | 2.2 | 4.60 x 10$^{-11}$ | 146 | 23000 |
| 20 nm | 2.2 | 5.60 x 10$^{-11}$ | 97 | 24000 |
| 30 nm | 2.2 | 5.30 x 10$^{-11}$ | 94 | 26000 |

| 40 nm | 2.2 | $5.60 \times 10^{-11}$ | 86 | 25000 |

## S2. Purification of the organic materials

All the tubes and container were made of quartz to avoid melting in high temperatures. An outer tube equipped with a pump system provides a high vacuum environment ($< 10^{-6}$ Torr). A container filled with a material of interest was place at the end of the inner tube and then loaded into the sublimation system. The position was controlled to place the material of interest in the first heating region. Elevates the temperature of first region over the sublimation point of the material of interest, the heavy impurities or non-vaporized substances remained in the container, while the remaining material become vapors and diffuse to a lower pressure, and, hence the region with lower temperatures. By carefully controlling the temperatures of these regions to form an appropriate thermal gradient, the material of interest and light impurities will deposit on the second and third region, respectively. After the sublimation process, a diamond tip tube cutter was used to cut the second region away from the first and third region to avoid mixing the impurities during the removal of the purified material.
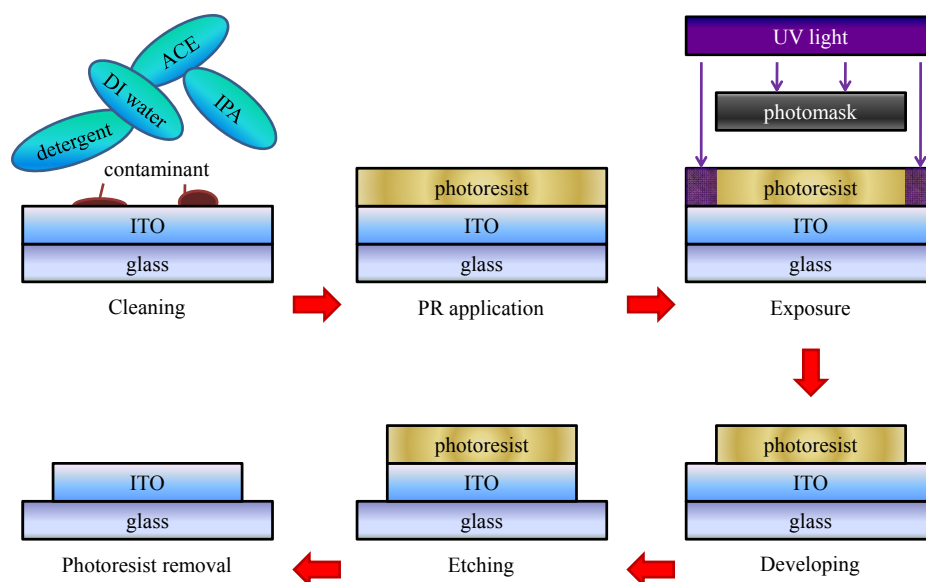


S3. Illustration of the home-build sublimation system for the organic materials.

## S3. The patterning process of ITO slides

The ITO substrates were soaked in consecutive solutions, detergent, deionized water, acetone, and isopropanol, and under ultrasonic bath in an ultrasonic cleaner (Delta DC200H) for 10 min each step. A positive photoresist (Everlight Chemical EPL 352) was used to cover the ITO substrate. The substrate then spun by a spin coater (M&R Nano Technology AGS-0206S) in a two-step approach (i.e., 550 rpm for 8 sec and 1250 rpm for 20 sec) to form a uniform layer. A hot plat (M&R Nano Technology YS-300S) was used to pre- and post-bake the substrates. The substrates were exposed to an UV light M&R Nano Technology AG350-6N-D-S-M-V) through a home-made photomask. The stripe-shaped photomask produced an image by blocking the area from UV exposure. The unexposed regions were soluble in a

developer (Everlgith Chemical EPD 1000) for 20 sec and left the undesirable area without protection of photoresist. The substrates then soaked in an etchant (Taiwan Maxwave ITO Etch-A1) for 15 min. The covered photoresist on the ITO slides were removed ultrasonic bath in acetone and isopropanol, thus producing the ITO slides studied here.



S4. Illustration of the patterning process for ITO slides. ACE, IPA, DI water denotes acetone, isopropanol, and deionized water respectively.

## S4. Device pattern and encapsulation

The device pattern is shown in the top view in Fig. S5. This layout design produced five OPV devices on the region overlapped between the ITO and metal films. The encapsulation process encased the organic layer with a UV-curable epoxy resin (Everwide, Taiwan) and a getter-attached glass covered on the top of the device, the side view of which is shown in Fig. S5. A syringe was used to spread the epoxy resin on the outside of the organic layer. A glass was then secured to the device with epoxy resin and gently depressed to compact the epoxy resin and eliminate the leaks. The encapsulation process was completed by curing the epoxy resin with UV illumination.
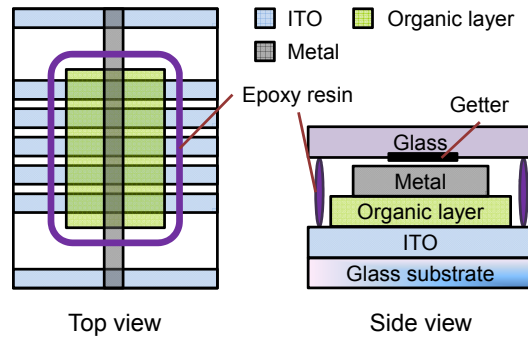
Fig. S5. Illustration of device pattern and encapsulation from top and side view.

**References**

1 S. Yoo, B. Domercq and B. Kippelen, *J. Appl. Phys.*, 2005, **97**, 103706.

2 W. J. Potscavage, S. Yoo and B. Kippelen, *Appl. Phys. Lett.*, 2008, **93**, 193308.

3 N. C. Giebink, G. P. Wiederrecht, M. R. Wasielewski and S. R. Forrest, *Phys. Rev. B*, 2010, **82**, 155305.